Author(s): Boraei, Ahmed T. A.; Haukka, Matti; Sarhan, Ahmed A. M.; Soliman, Saied M.; Al-Majid, Abdullah Mohammed; Barakat, Assem

Title: Synthesis and X-ray Crystal Structure of New Substituted 3-4'-Bipyrazole Derivatives : Hirshfeld Analysis, DFT and NBO Studies

Year: 2021

Version: Published version

crystals

MDPI

Article

Synthesis and X-ray Crystal Structure of New Substituted 3-4′-Bipyrazole Derivatives. Hirshfeld Analysis, DFT and NBO Studies

Ahmed T. A. Boraei [1,*], Matti Haukka [2], Ahmed A. M. Sarhan [3], Saied M. Soliman [4], Abdullah Mohammed Al-Majid [5] and Assem Barakat [5,*]

1 Chemistry Department, Faculty of Science, Suez Canal University, Ismailia 41522, Egypt
2 Department of Chemistry, University of Jyväskylä, P.O. Box 35, FI-40014 Jyväskylä, Finland; matti.o.haukka@jyu.fi
3 Chemistry Department, Faculty of Science, Arish University, Al-Arish 45511, Egypt; asarhan@aru.edu.eg
4 Department of Chemistry, Faculty of Science, Alexandria University, P.O. Box 426, Ibrahimia, Alexandria 21321, Egypt; saeed.soliman@alexu.edu.eg
5 Department of Chemistry, College of Science, King Saud University, P.O. Box 2455, Riyadh 11451, Saudi Arabia; amajid@ksu.edu.sa
* Correspondence: ahmed_boraei@science.suez.edu.eg (A.T.A.B.); ambarakat@ksu.edu.sa (A.B.); Tel.: +966-11467-5901 (A.T.A.B.); Fax: +966-11467-5992 (A.B.)

Abstract: A new compounds named 3-4′-bipyrazoles **2** and **3** were synthesized in high chemical yield from a reaction of pyran-2,4-diketone **1** with aryl hydrazines under thermal conditions in MeOH. Compound **2** was unambiguously confirmed by single-crystal X-ray analysis. It crystalizes in a triclinic crystal system and space group P-1. Its crystal structure was found to be in good agreement with the spectral characterizations. With the aid of Hirshfeld calculations, the H . . . H (54.8–55.3%) and H . . . C (28.3–29.2%) intermolecular contacts are the most dominant, while the O . . . H (5.8–6.5%), N . . . H (3.8–4.6%) and C . . . C (3.0–4.9%) are less dominant. The compound has a polar nature with a net dipole moment of 6.388 Debye. The BD(2)C31-C32→BD*(2)N4-C34 (27.10 kcal/mol), LP(1)N5→BD*(2)C31-C32 (36.90 kcal/mol), BD(1)C32-C34→BD*(1)C18-C31 (6.78 kcal/mol) and LP(1)N4→BD*(1)N5-C31 (7.25 kcal/mol) are the strongest π→π*, n→π*, σ-σ* and n→σ* intramolecular charge transfer processes, respectively.

Keywords: pyran-2,4-dione; bipyrazole; Hirshfeld analysis; NBO; DFT

Citation: Boraei, A.T.A.; Haukka, M.; Sarhan, A.A.M.; Soliman, S.M.; Al-Majid, A.M.; Barakat, A. Synthesis and X-ray Crystal Structure of New Substituted 3-4′-Bipyrazole Derivatives. Hirshfeld Analysis, DFT and NBO Studies. *Crystals* **2021**, *11*, 953. https://doi.org/10.3390/cryst11080953

Academic Editor: Paul R. Raithby

Received: 10 July 2021
Accepted: 13 August 2021
Published: 15 August 2021

1. Introduction

Pyranones are examples of ester-functional heterocyclic molecules which have been employed as a synthon for several targeted organic compounds [1]. These synthetic pyranones have been reported to have several applications related to medicine, including HIV protease inhibitors [2], anticonvulsants [3], antitumor [4,5], antifungal [3], and antimicrobial [6] agents, and as plant-growth regulators [2,7]. On the other hand, some other naturally occurring pyranones were reported to have interesting actions against bacteria, and also have cytotoxic effects (e.g., Marin natural product, Pectinatone) [8]. Another representative example works against inflammation and rheumatism (e.g., Bufalin) [9], and many others such as Pentylpyran-2-one [10] and Griseulin [11,12] exhibited antibiotic and mosquitocidal effects, respectively. These substituted pyranones scaffold have been studied extensively in the literature [13–15].

Heterocycles comprising five-membered rings with two adjacent nitrogen atoms are called pyrazoles, and these pharmacophore-containing heterocycles have been shown to have several therapeutic applications. They were reported to have interesting actions against different diseases, including cancer, inflammation, and bacterial infection, and can also be used as analgesic and antidepressant agents [16–18]. Pyrazolines are also

widely distributed in nature in the cells of animals and plants, and also exist in alkaloids, pigments, and vitamins [19]. Many approaches have been reported for the synthesis of pyrazoline scaffolds [20–26]. One representative common approach is a reaction of carbonyl compounds with hydrazines under thermal conditions [27], in addition to other reported methods for the synthesis of pyrazolines scaffold, such as the metal catalyzed approach [28].

In this context and continuation of our research program [29,30] here, we are reporting a facile and direct straightforward approach for the synthesis of substituted 3-4′-bipyrazoles in a catalyst free one-pot reaction, from pyran-2,4-dione and arylhydrazines. The structure of the newly synthesized 3-4′-bipyrazoles was confirmed by using different spectral characterizations. The X-ray structure of the bipyrazole **2** was further confirmed by single-crystal X-ray structure. Additionally, DFT calculations were used to predict its electronic parameters and calculate the different intramolecular charge transfer processes which stabilize the structure of **2**.

2. Materials and Methods

2.1. General

Melting points were measured using a melting-point apparatus (SMP10) in open capillaries and are uncorrected. The progress of the reaction was observed by thin-layer chromatography (TLC), and detection was achieved by UV light. Nuclear magnetic resonance (^{1}H- and ^{13}C-NMR) spectra were determined in DMSO-d_6 and were recorded on a Bruker AC 400 MHz spectrometer using tetramethylsilane as an internal standard. Chemical shifts are described in δ (ppm) and coupling constants are given in Hz. Elemental analysis was performed on a Flash EA-1112 instrument. X-ray crystallographic analysis was collected on a Rigaku Oxford Diffraction Supernova diffractometer using Cu Kα radiation. The UV-Vis electronic spectra were recorded in EtOH using a T90+UV/VIS spectrometer.

2.2. Synthesis of **2** *and* **3**

A methanolic solution of pyran-2,4-dione 1 (1.0 mmol) was mixed with phenylhydrazine or 4-chlorophenylhydrazine HCl (2.2 mmol) in methanol (10 mL), then the mixture was refluxed for 4 h. The resulting solutions were cooled to room temperature. The formed precipitates were collected by filtration and dried. Purifications were performed by recrystallization from EtOH in case of **2** and DCM/MeOH in case of **3**. Only good quality single crystals were obtained for **2**, which were found to be suitable for single-crystal X-ray diffraction analysis.

2.2.1. 2,2′,5,5′-Tetraphenyl-1′,2′-Dihydro-2H,3′H-[3,4′-Bipyrazol]-3′-One (**2**)

Yield: 88%, m.p. 270–271 °C. ^{1}H-NMR (400 MHz, DMSO-d_6) δ 12.01 (s, 1H), 7.99 (d, J = 7.6 Hz, 2H), 7.84 (d, J = 8.0 Hz, 2H), 7.53 (t, J = 7.6 Hz, 2H), 7.48 (t, J = 7.6 Hz, 2H),7.40–7.23 (m, 12H), 7.16 (s, 1H); ^{13}C-NMR (101 MHz, DMSO-d_6) δ 151.31, 140.28, 135.72, 133.33, 129.55, 129.30, 129.12, 128.79, 128.47, 127.57, 126.79, 126.59, 125.75, 124.21, 122.07, 108.40 (Figures S1 and S2 (Supplementary data)); CHN analysis for [$C_{30}H_{22}N_4O$] C, 79.27; H, 4.88; N, 12.33; O, 3.52 found C, 79.38; H, 4.99; N, 12.21. UV-Vis (EtOH): 264 nm (Figure S7 (Supplementary data)).

2.2.2. 2,2′-Bis(4-Chlorophenyl)-5,5′-Diphenyl-1′,2′-Dihydro-2H,3′H-[3,4′-Bipyrazol]-3′-One (**3**)

Yield: 61%, m.p. 227–228 °C. ^{1}H-NMR (400 MHz, DMSO-d_6) δ 12.25 (s, 1H), 7.97 (d, J = 7.6 Hz, 2H), 7.89 (d, J = 8.8 Hz, 2H), 7.60 (d, J = 8.8 Hz, 2H), 7.48(t, J = 7.6 Hz, 2H), 7.41–7.27 (m, 10H), 7.16 (s, 1H); ^{13}C-NMR (101 MHz, DMSO-d_6) δ 151.68, 138.97, 135.66, 133.04, 131.88, 130.34, 129.54, 129.33, 129.16, 129.04, 128.91, 128.83, 128.65, 126.67, 126.36, 125.80, 125.65, 123.35, 108.53 (Figures S3 and S4 (Supplementary data)); CHN analysis for

$[C_{30}H_{20}Cl_2N_4O]$ C, 68.84; H, 3.85; Cl, 13.55; N, 10.70 found C, 68.99; H, 3.86; Cl, 13.67; N, 10.62. UV-Vis (EtOH): 269 nm and 320 nm (Sh); (Figure S7 (Supplementary data)).

2.3. Crystal Structure Determination

The collecting experimental data for compound **2** are provided in the Supplementary Information.

2.4. Computational Study Protocols

All software and protocols employed for Hirshfeld surface analysis and DFT calculations are provided in the Supplementary Information.

3. Results and Discussion

3.1. Synthesis of **2** *and* **3**

In our recent publication [29], we reported that the pyran-2,4-diketone **1** could react with different amines and also amino acid esters to afford *β*-enaminones in a region-selective conversion. Interestingly, when pyran-2,4-dione **1** was reacted with aromatic hydrazines (phenylhydrazine and 4-chlorophenylhydrazine HCl) in MeOH under reflux conditions, the 3,4′-bipyrazol-3′-ones **2** and **3** were obtained. We assumed that the reaction occurred under a set of chemical transformations, including keto-enol tautomerism, aryl hydrazone formation, ring opening–closure, then keto-enol tautomerism, followed by aryl hydrazone formation with the second molecule of aryl hydrazine, and finally, ring closure upon the dehydration process (Scheme 1). The chemical structure of the final compounds was assigned based on various spectroscopic techniques (^{1}H- and ^{13}C-NMR, and CHN elemental analysis). Furthermore, compound **2** was unambiguously confirmed by single-crystal X-ray diffraction analysis.

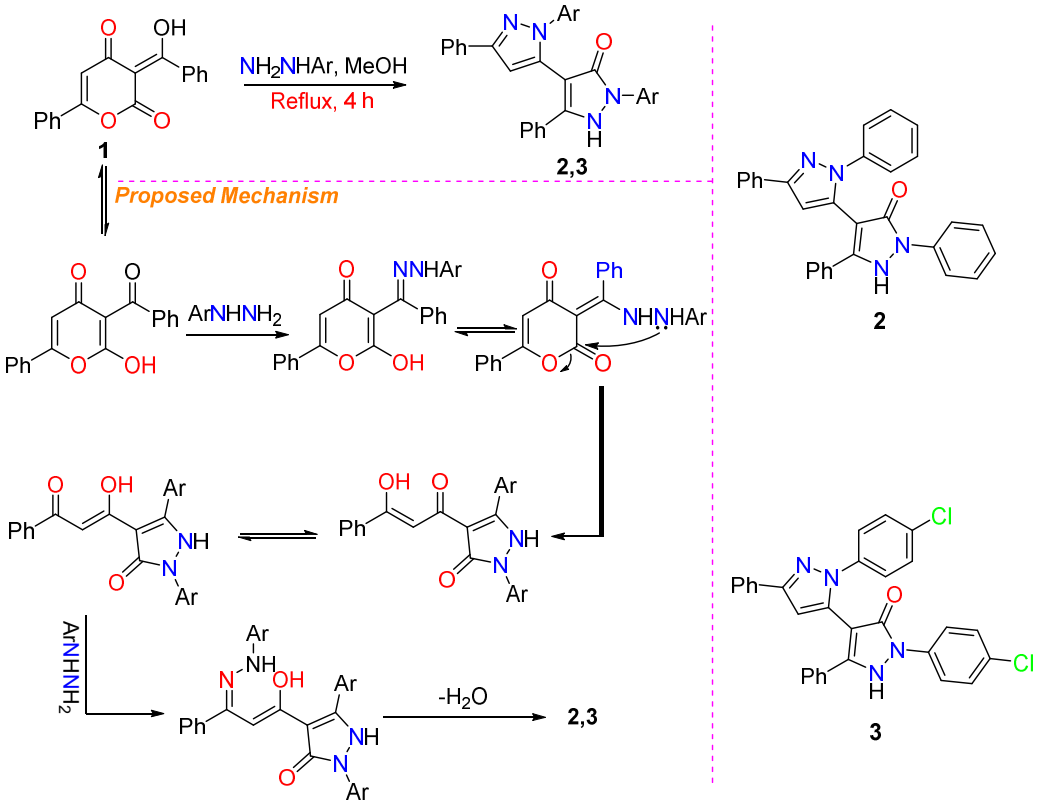

Scheme 1. Synthesis and proposed mechanism for compounds **2** and **3** starting from pyran-2,4-diketone **1**.

3.2. Crystal Structure Description of **2**

The X-ray structure of **2** is shown in Figure 1. The structure agreed very well with the spectral analyses. The crystal data and structure refinement details are depicted in Table 1. The compound crystallized in the triclinic system and P-1 space group with unit cell parameters of a = 11.0023(4) Å, b = 11.9332(5) Å, c = 18.0128(7) Å, α = 85.276(3)°, β = 84.517(3)° and γ = 85.240(3)°. The unit cell volume is 2339.40(16) Å^3 and Z = 4, and there are two molecules per asymmetric unit. Selected bond distances and angles are listed in Table 2.

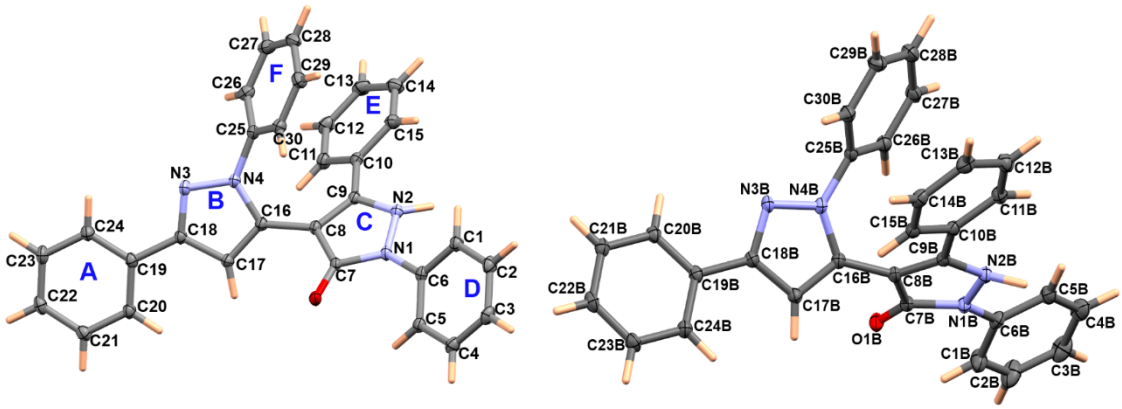

Figure 1. X-ray structure of **2**. Atom thermal ellipsoids are drawn at 30% probability level.

Table 1. Crystal Data for **2**.

	2
CCDC no.	2095217
empirical formula	$C_{30}H_{22}N_4O$
Fw	454.51
temp (K)	120(2)
λ(Å)	1.54184
cryst syst	Triclinic
space group	P?1
a (Å)	11.0023(4)
b (Å)	11.9332(5)
c (Å)	18.0128(7)
α(deg)	85.276(3)
β (deg)	84.517(3)
γ(deg)	85.240(3)
V (Å^3)	2339.40(16)
Z	4
ρ_{calc} (Mg/m^3)	1.290
μ(Mo Kα) (mm^{-1})	0.634
No. reflns.	17900
Unique reflns.	9577
Completeness to θ = 67.684° (%)	99.8
GOOF (F^2)	1.034
R_{int}	0.0419
R1 [a] ($I \geq 2\sigma$)	0.0485
wR2 [b] ($I \geq 2\sigma$)	0.1153

[a] $R1 = \Sigma \| \|F_o\| - \|F_c\| \| / \Sigma \|F_o\|$. [b] $wR2 = [\Sigma[w(F_o^2 - F_c^2)^2] / \Sigma[w(F_o^2)^2]]^{1/2}$.

Table 2. Selected bond lengths [Å] and angles [°] for **2**.

Atoms	Distance	Atoms	Distance
O1–C7	1.249(2)	O1B–C7B	1.250(2)
N1–N2	1.377(2)	N1B–N2B	1.387(2)
N1–C7	1.385(2)	N1B–C7B	1.395(2)
N1–C6	1.422(2)	N1B–C6B	1.410(2)
N2–C9	1.360(2)	N2B–C9B	1.354(2)
N3–C18	1.332(3)	N3B–C18B	1.345(2)
N3–N4	1.361(2)	N3B–N4B	1.366(2)
N4–C16	1.370(2)	N4B–C16B	1.365(2)
N4–C25	1.425(2)	N4B–C25B	1.431(2)
Atoms	**Angle**	**Atoms**	**Angle**
N2–N1–C7	110.01(15)	C5–C6–N1	118.42(17)
N2–N1–C6	121.68(15)	O1–C7–N1	123.25(16)
C7–N1–C6	127.14(15)	O1–C7–C8	131.41(17)
C9–N2–N1	107.80(15)	N1–C7–C8	105.28(15)
C18–N3–N4	104.58(15)	C9–C8–C7	107.45(16)
N3–N4–C16	112.08(15)	C9–C8–C16	130.99(17)
N3–N4–C25	120.64(16)	C7–C8–C16	121.41(16)
C16–N4–C25	127.25(16)	N2–C9–C8	109.10(16)
C6–C1–C2	118.41(19)	N2–C9–C10	119.81(16)
C3–C2–C1	120.4(2)	C8–C9–C10	130.96(17)
C2–C3–C4	120.37(19)	C15–C10–C11	119.13(19)
C3–C4–C5	120.4(2)	C15–C10–C9	120.99(17)
C4–C5–C6	118.60(19)	C11–C10–C9	119.84(17)
C1–C6–C5	121.75(18)	C12–C11–C10	120.09(19)
C1–C6–N1	119.82(18)		

The studied compound comprised six ring systems. The three rings **B**, **D** and **E** are twisted from the mean plane of ring **C** by 46.59, 36.61 and 30.90°, respectively. Similarly, rings **A** and **F** are twisted from ring **B** by 3.93 and 58.05°, respectively. The corresponding values of the second molecular unit are 58.02, 23.86, 24.74, 20.68 and 45.95°, respectively.

The molecules of **2** are connected with one another via strong N-H . . . O hydrogen bonding interactions. The hydrogen bond parameters are listed in Table 3 and presentation of the hydrogen bonding interactions among molecular units is shown in Figure 2 (upper part). In addition, the crystal structure of **2** comprised a large number of intra- and intermolecular π–π interactions. Summary of the short intra- and intermolecular C . . . C contacts are depicted in Table 4 and shown in the lower part of Figure 2.

Table 3. Hydrogen bonds for **2** [Å and °].

D-H . . . A	d(D-H)	d(H . . . A)	d(D . . . A)	<(DHA)
N2-H2 . . . O1B	0.95(3)	1.73(3)	2.681(2)	173(3)
N2B-H2B . . . O1 #1	1.01(3)	1.65(3)	2.648(2)	166(3)

#1 x + 1,y,z.

Table 4. The intra- and intermolecular π-π interactions for **2** [Å].

Contact	Distance	Contact	Distance
C8 . . . C30	3.195	C8B . . . C26B	3.127
C9 . . . C25	3.287	C9B . . . C25B	3.342
C9 . . . C30	3.316	C9B . . . C26B	3.296
C10 . . . C25	3.307	C10B . . . C25B	3.331
C11 . . . C16	3.303	C15B . . . C16B	3.142
C11 . . . C26	3.335	C15B . . . C25B	3.336
C4 . . . C26B	3.264	C4 . . . C4	3.273 [ii]
C24 . . . C24	3.39 [i]	C21 . . . C14B	3.369 [iii]

Symm. Codes: [i] −1 − x,−y,2 − z; [ii] −x,1 − y,1 − z; [iii] −x,1 − y,1 − z.

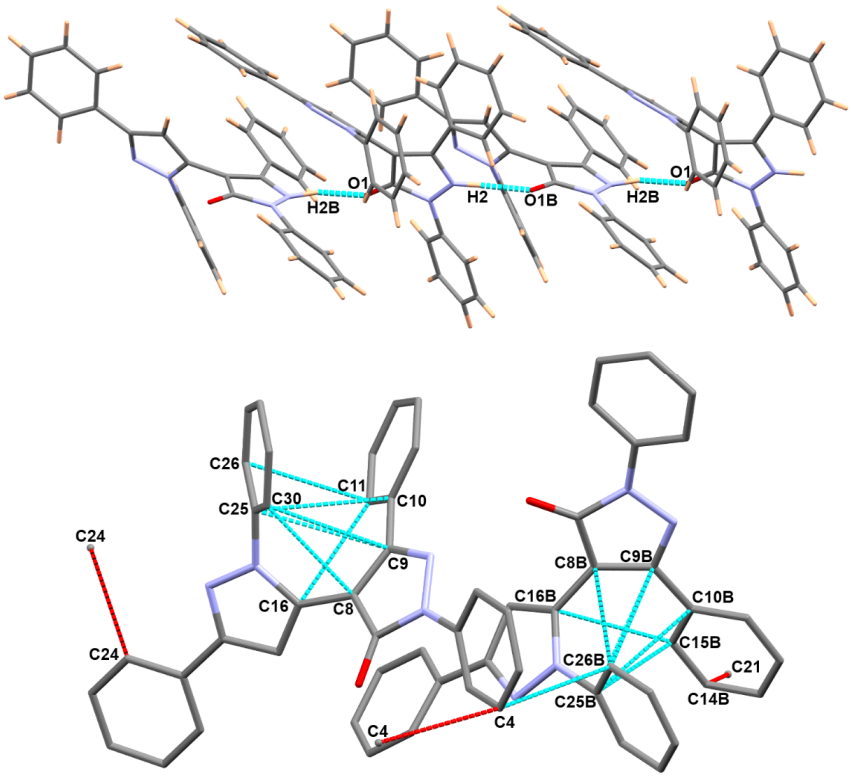

Figure 2. Packing of molecular units via N-H . . . O H-bonding interactions (**upper**) and the important intra- and intermolecular π–π stacking interactions (**lower**).

3.3. Analysis of Molecular Packing

The Hirshfeld surfaces, including the d_{norm}, shape index and curvedness maps of **2** are shown in Figure 3. In the d_{norm} map, there are many short distance contacts appearing as red spots. In the studied crystal, there are two molecular units per asymmetric formula; hence, the Hirshfeld results are discussed for the two molecular units.

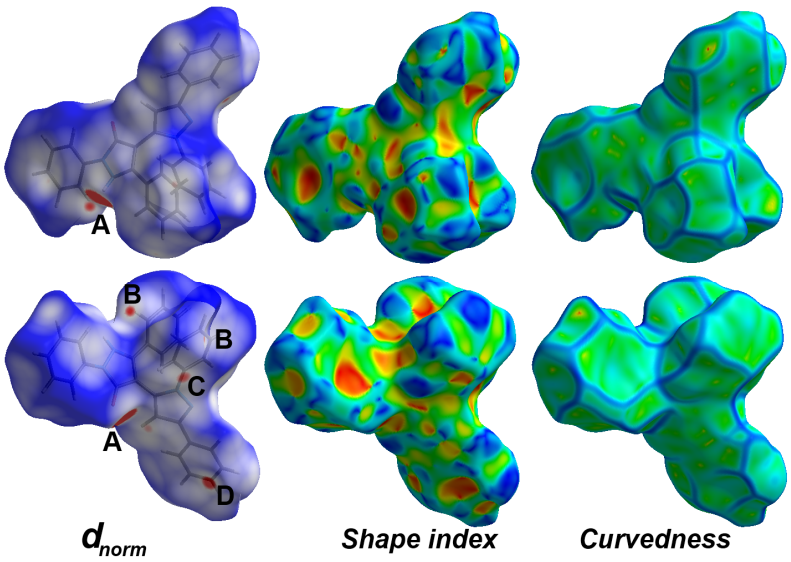

Figure 3. Hirshfeld surfaces for the molecular unit with atom numbering comprising **B** of **2**. The results for the other unit are presented in Figure S5 (Supplementary data). **A:** O . . . H, **B:** H . . . H, **C:** C . . . C and **D:** H . . . C contacts.

The decomposition of all possible contacts with the aid of fingerprint plots gave the percentages of all intermolecular interactions controlling the molecular packing of **2** (Figure 4). It is clear that the H . . . H and H . . . C interactions are the most dominant, which comprised 54.8–55.3% and 28.3–29.2% of the whole fingerprint area. The other contacts such as O . . . H (5.8–6.5%), N . . . H (3.8–4.6%) and C . . . C (3.0–4.9%) are less dominant in the crystal structure of **2**. A summary of all possible contacts in both units are presented in Figure 5.

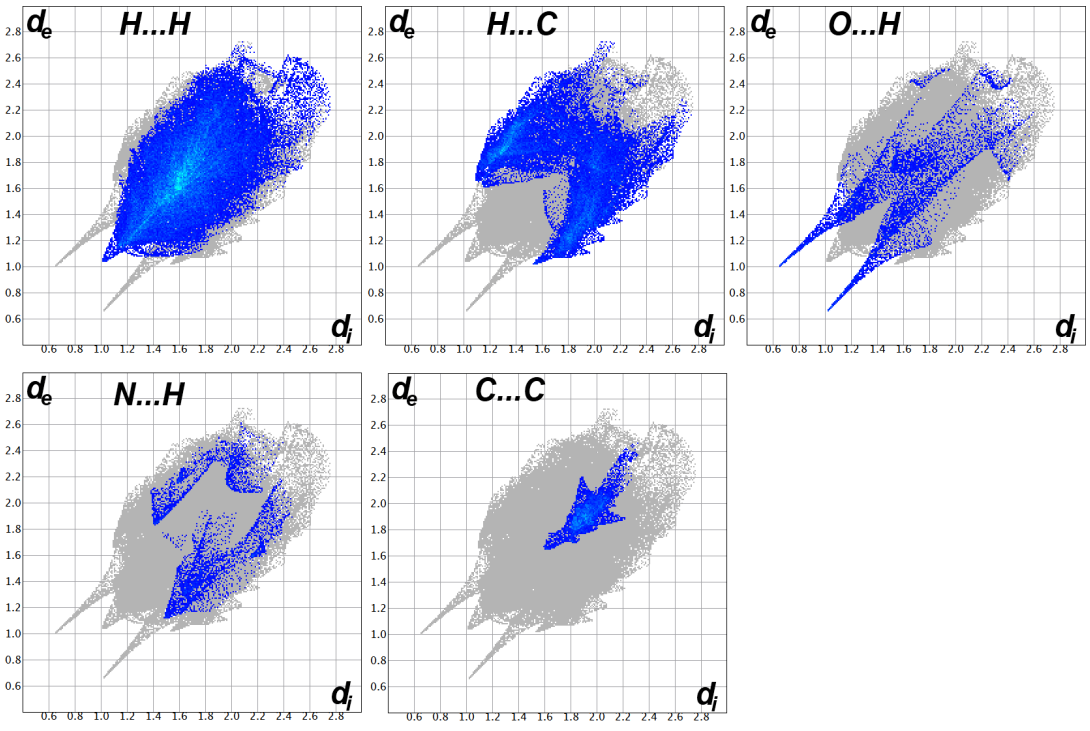

Figure 4. Decomposed fingerprint plots for the molecular unit with atom numbering comprising **B**. The results for the other unit are presented in Figure S6 (Supplementary data).

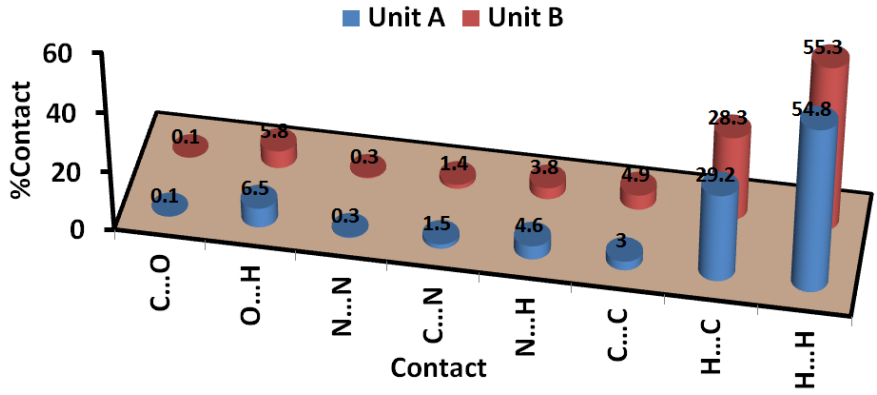

Figure 5. The percentages of all possible intermolecular interactions in the crystal structure of **2**.

For simplicity, the most important short contacts are labelled **A** to **D** in the d_{norm} map shown in Figure 3. These red spots represent the intermolecular interactions with shorter distances than the van der Waals radii sum of the interacting atoms. The interaction distances of these short contacts are summarized in Table 5. The O ... H hydrogen bonds are significantly shorter. The O1B ... H2 and O1 ... H2B contacts have contact distances of 1.677 and 1.658 Å, respectively. In contrast, the H ... C interactions are significantly longer with interaction distances ranging from 2.559 Å (H17 ... C21B) to 2.776 Å (H30 ... C4B). On the other hand, the shortest H ... H and C ... C contacts are H3 ... H11B and C4 ... C26B with interaction distances of 2.056 and 3.264Å, respectively. These intermolecular interactions have an important role in the stability of the crystalline structure of the studied compound.

Table 5. Most important contacts and the corresponding shortest interaction distances.

Contact	Distance	Contact	Distance
O1B ... H2	1.677	H30 ... C4B	2.776
O1 ... H2B	1.658	H2 ... C7B	2.613
O1 ... H5B	2.465	H12B ... C28	2.761
H23 ... C12	2.726	H2B ... C7	2.608
H14B ... C21	2.769	H3 ... H11B	2.056
H17 ... C21B	2.559	C4 ... C26B	3.264

3.4. DFT Studies

The structure of **2** was optimized and the resulting minimum energy structure was shown in Figure 6. An overlay of the calculated structure with the experimental one is presented in the same figure. There are good agreements between the calculated bond distances and angles with the experimental ones (Table S1, Supplementary data). In Figure 7, there are excellent straight-line correlations (R^2 = 0.906–0.951) between the calculated and experimental geometric parameters. Little variation between the calculated and experimental structures could be attributed to the crystal packing effects.

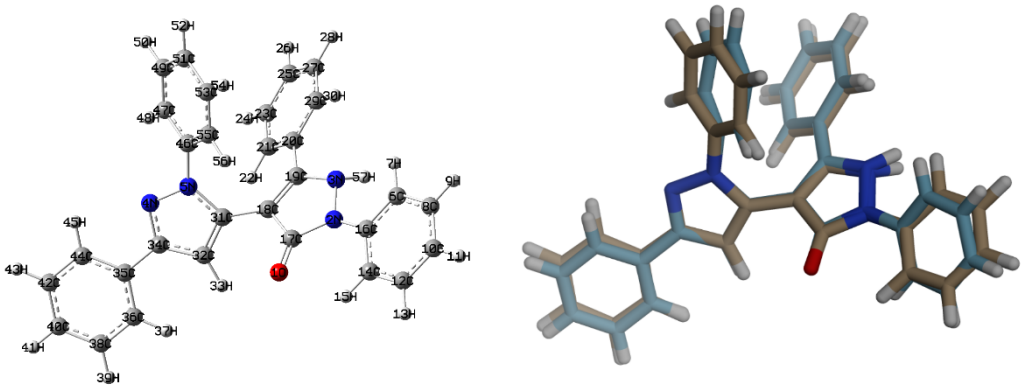

Figure 6. The calculated geometry (**left**) and its overlay with the experimental one, (**right**) for **2**. For the experimental model used for the comparison with the optimized one, see Figure 1 (left part).

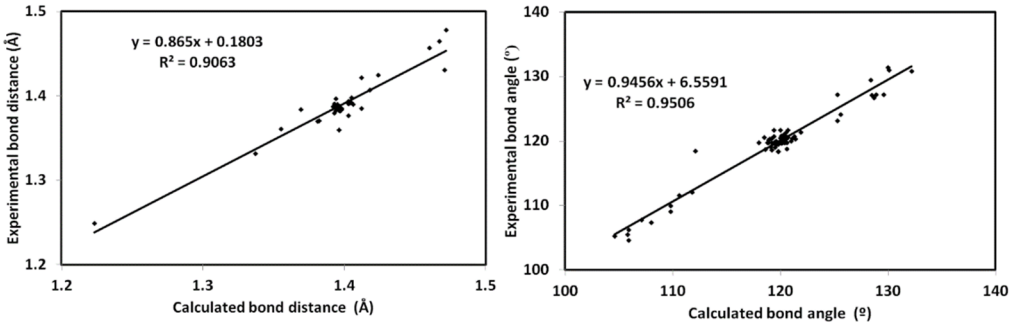

Figure 7. The correlations between the calculated and experimental geometric parameters.

The distribution of charges at the different atomic sites was predicted with the aid of natural population analysis (Figure 8). The results indicated the high electronegative nature of the nitrogen and oxygen atoms. Their natural charges were calculated to be −0.6160 and −0.1673 to −0.4294 e, respectively. Additionally, all carbons are negatively charged except those bonded to electronegative atoms. In contrast, all hydrogen atoms are electropositive. Of these atomic sites, the NH proton (0.427 e) and the carbonyl carbon (0.655 e) are the most electropositive. The studied molecule is highly polar with a net dipole moment of 6.388 Debye, and the direction of the dipole moment vector is presented in Figure 9.

In the MEP map shown in the right part of Figure 9, there is an intense red region found close to the carbonyl oxygen atom, while a blue region is close to the NH proton, which represent molecular sites with the highest and lowest electron density, respectively. Hence, the carbonyl oxygen atom and the NH proton are the most probable sites as hydrogen bond acceptors and donors, respectively. This analysis is in accord with the observed X-ray structure of the studied system. In Figure 9, the HOMO and LUMO levels are also presented. It is clear that the HOMO and LUMO are mainly located over the delocalized π system of the compound. Hence, the HOMO–LUMO intramolecular charge transfer could be described as π–π* transition.

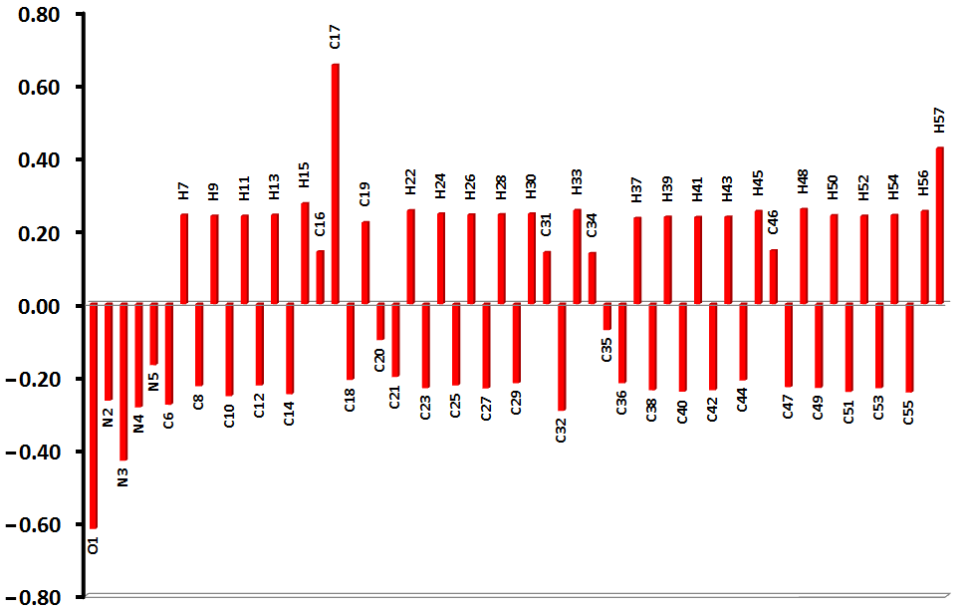

Figure 8. Natural charge distributions in **2**.

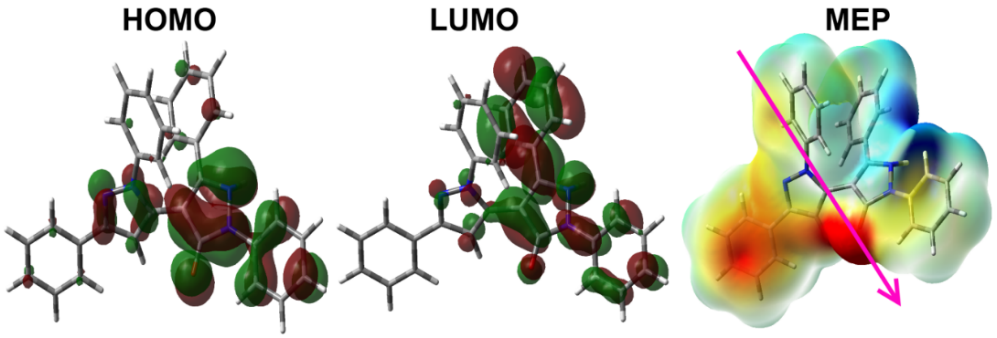

Figure 9. The MEP, HOMO and LUMO of **2**. In molecular electrostatic potential (MEP): red (most negative) and blue (most positive).

Based on the HOMO and LUMO energies, the ionization potential ($I = -E_{HOMO}$), electron affinity ($A = -E_{LUMO}$), chemical potential ($\mu = -(I + A)/2$), hardness ($\eta = (I - A)/2$), as well as electrophilicity index ($\omega = \mu^2/2\eta$) were calculated [31–37]. These reactivity indices are calculated to be 5.571, 1.645, −3.608, 3.926, and 1.658 eV, respectively. It was believed that these electronic parameters have important rule in the biomolecular reactivity.

3.5. NBO Analysis

The stabilization of molecular systems through electron delocalization from occupied orbitals to antibonding empty orbitals was investigated using NBO calculations [38,39]. The results of the stabilization energies ($E^{(2)}$) due to the different electron delocalization processes are summarized in Table 6. The compound is stabilized by a large number of $\pi \rightarrow \pi^*$ intramolecular charge transfer (IMCT) processes. The strongest $\pi \rightarrow \pi^*$ IMCT processes is BD(2)C31-C32→BD*(2)N4-C34, which stabilized the structure by 27.10 kcal/mol. The structure is also stabilized by a number of strong $n \rightarrow \pi^*$ IMCT processes which stabilized the system up to 36.90 kcal/mol for the LP(1)N5→BD*(2)C31-C32 IMCT process. In contrast, the σ–σ^* and $n \rightarrow \sigma^*$ IMCT processes stabilized the system to weaker extents. The BD(1)C32-C34→BD*(1)C18-C31 (6.78 kcal/mol) and LP(1)N4→BD*(1)N5-C31 (7.25 kcal/mol) are the strongest σ–σ^* and $n \rightarrow \sigma^*$ IMCT in the studied molecule.

Table 6. The $E^{(2)}$ (kcal/mol) values for the IMCT interactions in **2**[a].

NBO [i]	NBO [j]	$E^{(2)}$	Donor NBO [i]	Acceptor NBO [j]	$E^{(2)}$
BD(1) C17–C18	BD*(1) C19–C20	6.61	BD(2) N4–C34	BD*(2) C31–C32	12.59
BD(1) C18–C31	BD*(1) C18–C19	5.00	BD(2) N4–C34	BD*(2) C35–C36	9.42
BD(1) C31–C32	BD*(1) N5–C46	5.06	BD(2) C6–C16	BD*(2) C8–C10	20.71
BD(1) C31–C32	BD*(1) C34–C35	5.39	BD(2) C6–C16	BD*(2) C12–C14	17.34
BD(1) C32–C34	BD*(1) C18–C31	6.78	BD(2) C8–C10	BD*(2) C6–C16	19.45
			BD(2) C8–C10	BD*(2) C12–C14	20.87
LP(1) N4	BD*(1) N5–C31	7.25	BD(2) C12–C14	BD*(2) C6–C16	21.86
LP(1) N4	BD*(1) C32–C34	5.38	BD(2) C12–C14	BD*(2) C8–C10	19.25
			BD(2) C18–C19	BD*(2) C20–C29	7.95
LP(1) N2	BD*(2) C6–C16	29.57	BD(2) C18–C19	BD*(2) C31–C32	5.57
LP(1) N3	BD*(2) C18–C19	20.16	BD(2) C20–C29	BD*(2) C18–C19	13.95
LP(1) N5	BD*(2) N4–C34	28.45	BD(2) C20–C29	BD*(2) C21–C23	19.16
LP(1) N5	BD*(2) C31–C32	36.90	BD(2) C20–C29	BD*(2) C25–C27	19.32
LP(1) N5	BD*(2) C46–C55	17.17	BD(2) C21–C23	BD*(2) C20–C29	19.89
			BD(2) C21–C23	BD*(2) C25–C27	20.53
			BD(2) C25–C27	BD*(2) C20–C29	21.42
			BD(2) C25–C27	BD*(2) C21–C23	19.25
			BD(2) C31–C32	BD*(2) N4–C34	27.10
			BD(2) C31–C32	BD*(2) C18–C19	6.37
			BD(2) C35–C36	BD*(2) N4–C34	20.01
			BD(2) C35–C36	BD*(2) C38–C40	20.92
			BD(2) C35–C36	BD*(2) C42–C44	19.13
			BD(2) C38–C40	BD*(2) C35–C36	19.85
			BD(2) C38–C40	BD*(2) C42–C44	19.52
			BD(2) C42–C44	BD*(2) C35–C36	19.90
			BD(2) C42–C44	BD*(2) C38–C40	20.31
			BD(2) C46–C55	BD*(2) C47–C49	19.29
			BD(2) C46–C55	BD*(2) C51–C53	20.04
			BD(2) C47–C49	BD*(2) C46–C55	20.93
			BD(2) C47–C49	BD*(2) C51–C53	20.13
			BD(2) C51–C53	BD*(2) C46–C55	20.39
			BD(2) C51–C53	BD*(2) C47–C49	20.21

[i] Donor; [j] Acceptor.

4. Conclusions

In conclusion, newly substituted 3-4′-bipyrazoles were synthesized for the first time using a simple one-pot method from pyran-2,4-diketone and arylhydrazines. The structure of the newly synthesized compounds were elucidated using elemental analysis and spectroscopic techniques. The supramolecular structure of the crystallized compound **2** was analyzed using Hirshfeld calculations. Moreover, the optimized geometry calculations showed good agreement with the experimental data. Different electron delocalization processes which stabilized the system through conjugation effects were also calculated using natural bond orbital calculations. HOMO, LUMO and MEP as well as the electronic reactivity descriptors were also presented and discussed.

Supplementary Materials: The following are available online at https://www.mdpi.com/article/10.3390/cryst11080953/s1, X-Ray single-crystal determination of **2**; Table S1: The calculated geometric parameters of **2**, Figure S1–S4. ^{1}H- and ^{13}C-NMR for compounds **2** and **3** in DMSO-d_6, Figure S5. Hirshfeld surfaces for the other molecular unit in the crystal structure of **2**; Figure S6. Decomposed fingerprint plots for the other molecular unit the crystal structure of **2**; Figure S7. Uv-Vis spectra of compounds **2** and **3.**

Author Contributions: Conceptualization, A.T.A.B., S.M.S. and A.B.; synthesis and characterization, A.T.A.B., A.A.M.S. and A.M.A.-M.; X-ray crystal structure was carried out by: M.H.; writing—original manuscript, A.T.A.B., S.M.S. and A.B.; revision and editing, A.T.A.B., S.M.S. and A.B. All authors have read and agreed to the published version of the manuscript.

Funding: Researchers Supporting Project (RSP-2021/64), King Saud University, Riyadh, Saudi Arabia.

Institutional Review Board Statement: Not applicable.

Informed Consent Statement: Not applicable.

Data Availability Statement: Not applicable.

Acknowledgments: The authors would like to extend their sincere appreciation to the Researchers Supporting Project (RSP-2021/64), King Saud University, Riyadh, Saudi Arabia.

Conflicts of Interest: The authors declare no conflict of interest.

References

1. Lee, J.S. Recent advances in the synthesis of 2-pyrones. *Mar. Drugs* **2015**, *13*, 1581–1620. [CrossRef]
2. Fisch, M.H.; Flick, B.H.; Arditti, J. Structure and antifungal activity of hircinol, loroglossol and orchinol. *Phytochemistry* **1973**, *12*, 437–441. [CrossRef]
3. Kelly, T.R.; Li, Q.; Bhushan, V. Intramolecular biaryl coupling: Asymmetric synthesis of the chiral B-ring diol unit of pradimicinone. *Tetrahedron Lett.* **1990**, *31*, 161–164. [CrossRef]
4. Boger, D.L.; Mullican, M.D. Regiospecific total synthesis of juncusol. *J. Org. Chem.* **1984**, *49*, 4045–4050. [CrossRef]
5. Rabideau, P.W.; Harvey, R.G. Metal-ammonia reduction. VII. Stereospecific re- duction in the phenanthrene series. *J. Org. Chem.* **1970**, *35*, 25–30. [CrossRef]
6. Goel, A.; Ram, V.J. Natural and synthetic 2 *H*-pyran-2-ones and their versatility in organic synthesis. *Tetrahedron* **2009**, *65*, 7865–7913. [CrossRef]
7. Tsuchiya, K.; Kobayashi, S.; Nishikiori, T.; Nakagawa, T.; Tatsuta, K. NK10958P, a novel plant growth regulator produced by Streptomyces sp. *J. Antibiot.* **1997**, *50*, 259–260. [CrossRef]
8. Birkbeck, A.A.; Enders, D. The total synthesis of (+)-pectinatone: An iterative alkylation approach based on the SAMP-hydrazone method. *Tetrahedron Lett.* **1998**, *39*, 7823–7826. [CrossRef]
9. Costa, S.S.; Jossang, A.; Bodo, B. 4′′′′-Acetylsagittatin A, a kaempferol triglycoside from Kalanchoe streptantha. *J. Nat. Prod.* **1996**, *59*, 327–329. [CrossRef]
10. Parker, S.R.; Cutler, H.G.; Jacyno, J.M.; Hill, R.A. Biological activity of 6-pentyl-2-*H*-pyran-2-one and its analogs. *J. Agric. Food Chem.* **1997**, *45*, 2774–2776. [CrossRef]
11. Nair, M.G.; Chandra, A.; Thorogood, D.L. Griseulin, a new nitro-containing bioactive metabolite produced by Streptomyces spp. *J. Antibiot.* **1993**, *46*, 1762–1763. [CrossRef]
12. Ishibashi, Y.; Nishiyama, S.; Yamamura, S. Structural revision of griseulin, a bioactive pyrone possessing a nitrophenyl unit. *Chem. Lett.* **1994**, 1747–1748. [CrossRef]
13. Xue, F.; Li, X.; Wan, B. A class of benzene backbone-based olefin-sulfoxide ligands for Rh-catalyzed enantioselective addition of arylboronic acids to enones. *J. Org. Chem.* **2011**, *76*, 7256–7262. [CrossRef]
14. Gianni, J.; Pirovano, V.; Abbiati, G. Silver triflate/p-TSA co-catalysed synthesis of 3-substituted isocoumarins from 2-alkynylbenzoates. *Org. Biomol. Chem.* **2018**, *16*, 3213–3219. [CrossRef] [PubMed]
15. Hosny, M.; Fawzy, M.; Abdelfatah, A.M.; Fawzy, E.E.; Eltaweil, A.S. Comparative study on the potentialities of two halophytic species in the green synthesis of gold nanoparticles and their anticancer, antioxidant and catalytic efficiencies. *Adv. Powder Technol.* **2021**, in press. [CrossRef]
16. Shaaban, M.R.; Mayhoub, A.S.; Farag, A.M. Recent advances in the therapeutic applications of pyrazolines. *Expert. Opin. Ther. Pat.* **2012**, *22*, 253–291. [CrossRef] [PubMed]
17. Varghese, B.; Al-Busafi, S.N.; Suliman, F.O.; Al-Kindy, S.M.Z. Unveiling a versatile heterocycle: Pyrazoline—A review. *RSC Adv.* **2017**, *7*, 46999–47016. [CrossRef]
18. Tok, F.; Abas, B.I.; Çevik, O.; Koçyiğit-Kaymakçıoğlu, B. Design, synthesis and biological evaluation of some new 2-pyrazoline derivatives as potential anticancer agents. *Bioorg. Chem.* **2020**, *102*, 104063. [CrossRef]
19. Yusuf, M.; Jain, P. Synthetic and biological studies of pyrazolines and related heterocyclic compounds. *Arab. J. Chem.* **2014**, *7*, 553–596. [CrossRef]
20. Kariuki, B.M.; Abdel-Wahab, B.F.; El-Hiti, G.A. Synthesis and structural characterization of isostructural 4-(4-Aryl)-2-(5-(4-fluorophenyl)-3-(1-(4-fluorophenyl)-5-methyl-1*H*-1,2,3-triazol-4-yl)-4,5-dihydro-1*H*-pyrazol-1-yl)thiazoles. *Crystals* **2021**, *11*, 795. [CrossRef]
21. Mabkhot, Y.N.; Al-Majid, A.M.; Barakat, A.; Alshahrani, S.; Siddiqui, Y. 1,1′-(3-Methyl-4-phenylthieno[2,3-*b*]thiophene-2,5-diyl)diethanone as building block in heterocyclic synthesis. Novel synthesis of some pyrazoles, and pyrimidines derivatives. *Molecules* **2011**, *16*, 6502–6511. [CrossRef]
22. Mabkhot, Y.N.; Barakat, A.; Al-Majid, A.M.; Al-Othman, Z.A.; Alamary, A.S. A Facile and convenient synthesis of some novel hydrazones, schiff's base and pyrazoles incorporating thieno [2,3-*b*]thiophenes. *Int. J. Mol. Sci.* **2011**, *12*, 7824–7834. [CrossRef]

23. Mabkhot, Y.N.; Kaal, N.A.; Alterary, S.; Al-Showiman, S.S.; Barakat, A.; Ghabbour, H.A.; Frey, W. Synthesis, in-vitro antibacterial, antifungal, and molecular modeling of potent anti-microbial agents from a combined pyrazole and thiophene pharmacophore. *Molecules* **2015**, *20*, 8712–8729. [CrossRef]
24. Elshaier, Y.A.M.M.; Barakat, A.; Al-Qahtany, B.M.; Al-Majid, A.M.; Al-Agamy, M.H. Synthesis of pyrazole-thiobarbituric acid derivatives: Antimicrobial activity and docking studies. *Molecules* **2016**, *21*, 1337. [CrossRef] [PubMed]
25. Barakat, A.; Al-Qahtani, B.M.; Al-Majid, A.M.; Ali, M.; Mabkhot, Y.N.; Al-Agamy, M.H.M.; Wadood, A. Synthesis, characterization, anti-microbial activity and molecular docking studies of combined pyrazol-barbituric acid pharmacophore. *Trop. J. Pharm. Res.* **2016**, *15*, 1319–1326. [CrossRef]
26. Barakat, A.; Al-Majid, A.; Al-Qahtani, B.M.; Ali, M.; Teleb, M.; Al-Agamy, M.H.M.; Naz, S.; Ul-Haq, Z. Synthesis, antimicrobial activity, pharmacophore modeling and molecular docking studies of new pyrazole-dimedone hybrid architectures. *Chem. Cent. J.* **2018**, *12*, 29. [CrossRef]
27. Lellek, V.; Chen, C.-Y.; Yang, W.; Liu, J.; Ji, X.; Faessler, R. An efficient synthesis of substituted pyrazoles from one-pot reaction of ketones, aldehydes, and hydrazine monohydrochloride. *Synlett* **2018**, *29*, 1071–1075. [CrossRef]
28. Alex, K.; Tillack, A.; Schwarz, N.; Beller, M. Zinc-catalyzed synthesis of pyrazolines and pyrazoles via hydrohydrazination. *Org. Lett.* **2008**, *10*, 2377–2379. [CrossRef] [PubMed]
29. Sarhan, A.A.M.; Haukka, M.; Barakat, A.; Boraei, A. A novel synthetic approach to pyran-2,4-dione scaffold production:Microwave-assisted dimerization, cyclization, and expeditiousregioselective conversion intob-enamino-pyran-2,4-diones. *Tetrahedron Lett.* **2020**, *61*, 152660. [CrossRef]
30. Boraei, A.T.A.; Haukka, M.; Sarhan, A.A.M.; Soliman, S.M.; Barakat, A. Intramolecular hydrogen bond, hirshfeld analysis, AIM; DFT studies of pyran-2,4-dione derivatives. *Crystals* **2021**, *11*, 896. [CrossRef]
31. Foresman, J.B.; Frisch, E. *Exploring Chemistry with Electronic Structure Methods*, 2nd ed.; Gaussian: Pittsburgh, PA, USA, 1996.
32. Chang, R. *Chemistry*, 7th ed.; McGraw-Hill: New York, NY, USA, 2001.
33. Kosar, B.; Albayrak, C. Spectroscopic investigations and quantum chemical computational study of (E)-4-methoxy-2-[(p-tolylimino) methyl] phenol. *Spectrochim. Acta* **2011**, *78*, 160–167. [CrossRef] [PubMed]
34. Koopmans, T.A. Ordering of wave functions and eigenenergies to the individual electrons of an atom. *Physica* **1933**, *1*, 104–113. [CrossRef]
35. Parr, R.G.; Yang, W. *Density-Functional Theory of Atoms and Molecules*; Oxford University Press: New York, NY, USA, 1989.
36. Parr, R.G.; Szentpaly, L.V.; Liu, S. Electrophilicity index. *J. Am. Chem. Soc.* **1999**, *121*, 1922–1924. [CrossRef]
37. Singh, R.N.; Kumar, A.; Tiwari, R.K.; Rawat, P.; Gupta, V.P. A combined experimental and quantum chemical (DFT and AIM) study on molecular structure, spectroscopic properties, NBO and multiple interaction analysis in a novel ethyl 4-[2-(carbamoyl) hydrazinylidene]-3, 5-dimethyl-1H-pyrrole-2-carboxylate and its dimer. *J. Mol. Strut.* **2013**, *1035*, 427–440. [CrossRef]
38. Joe, I.H.; Kostova, I.; Ravikumar, C.; Amalanathan, M.; Pinzaru, S.C. Theoretical and vibrational spectral investigation of sodium salt of acenocoumarol. *J. Raman Spectrosc.* **2009**, *40*, 1033–1038.
39. Sebastian, S.; Sundaraganesan, N. The spectroscopic (FT-IR, FT-IR gas phase, FT-Raman and UV) and NBO analysis of 4-Hydroxypiperidine by density functional method. *Spectrochim. Acta Part A Mol. Biomol. Spectrosc.* **2010**, *75*, 941–952. [CrossRef]